Adaptive Prescribed-Time Agile Control for Hypersonic Morphing Vehicles

Gu Xin, Wei Changzhu, Huang Hao and Zhang Yuhao*

School of Astronautics, Harbin Institute of Technology, Harbin 150001, China

Abstract: For the agile control of hypersonic morphing vehicles during high-maneuverability flight, an adaptive prescribed-time agile control method is proposed. To address model mismatch and agile control challenges arising from unsteady aerodynamic characteristics during high-maneuver hypersonic variable-shape vehicles, an adaptive prescribed-time agile control method is proposed. This approach employs prescribed-time sliding mode control as the baseline controller, integrated with adaptive dynamic programming to reduce the theoretical upper bound of prescribed time while enhancing agility. Furthermore, through non-singular control input design, the method maintains the specified time-constrained implementation while preserving the predetermined ratio between system bandwidth and actuator bandwidth. Based on Lyapunov theory, the stability of the closed-loop controller was demonstrated. Finally, a set of comparative simulations demonstrates that the proposed control method achieves prescribed-time convergence while exhibiting lower conservatism, stronger model adaptability, and higher control accuracy. Additionally, the controller possesses input optimization capabilities that significantly reduce the torque required for computation.

Keywords: Hypersonic Morphing Vehicles, Prescribed-time Control, Adaptive Dynamic Programming, Sliding Mode Control.

1. INTRODUCTION

Hypersonic vehicles operate across an extremely wide range of airspeeds, making it difficult for a single aerodynamic configuration to achieve optimal performance throughout the entire flight envelope. Consequently, the concept of hypersonic morphing vehicle has emerged [1]. By dynamically adjusting its physical configuration, a hypersonic morphing vehicle achieves a high degree of adaptation to variable environments and mission conditions [2]. Control system stability is a necessary condition for such a vehicle to accomplish its flight missions. However, morphing induces significant changes in parameters such as the vehicle's center of mass, moment of inertia, and aerodynamic coefficients. Furthermore, the hypersonic flight process involves large maneuvers and is subject to strong disturbances, which exacerbate the impact of these parameter variations on the control system, posing significant challenges for control system design [3]. On one hand, this results in a highly nonlinear vehicle model, and the unsteady aerodynamic characteristics induced by morphing are difficult to model offline. On the other hand, it significantly alters the response characteristics of the vehicle system, leading to variations in the system bandwidth. This makes it difficult to maintain the designed ratio between the controller bandwidth and the vehicle system bandwidth [4-6].

Control methods based on linearization have achieved good performance in fixed-configuration vehicle control and have been extended to morphing vehicle controller design. Such research focuses on handling the strongly time-varying, nonlinear dynamics arising from aerodynamic shape changes during the morphing process to maintain flight stability. He *et al*. constructed a morphing vehicle model based on tensor products and designed an LPV control system using parallel distributed compensation control technology and regional pole placement, achieving stable command tracking during morphing [7]. Yue *et al*., focusing on a tailless folding-wing morphing vehicle, obtained an LPV model through linearization and designed a gain-scheduled H∞ robust controller for the wing transformation process to ensure robust stability of the time-varying dynamics. Simulation results showed the controller could maintain stability throughout the morphing process [8]. Wang *et al*., for a variable-sweep vehicle, divided the range of time-varying parameters into several regions. Utilizing weighting coefficients and the concept of parameter overlap regions, they constructed a set of LPV controllers by solving linear matrix inequalities and designed a controller switching strategy with sweep angle as the decision variable, enabling good disturbance rejection during morphing [9]. Wu *et al*. derived an LPV model with wingspan and sweep angle as time-varying parameters and introduced an adaptation law to enhance the robustness of a sliding mode controller [10].

However, methods based on linearization essentially utilize finite approximation of nonlinear

*Address correspondence to this author at the School of Astronautics, Harbin Institute of Technology, Harbin 150001, China;
E-mail: weichangzhu@hit.edu.cn

characteristics near local equilibrium points, while morphing vehicle models are highly nonlinear, and the morphing process exhibits significant unsteady aerodynamic characteristics. This can easily lead to overly conservative controller designs based on linearization, degrading dynamic performance [11]. Especially for hypersonic vehicles during large maneuvers, high dynamic pressure and strong disturbances exacerbate this issue, potentially causing control model mismatch and frequent actuator saturation, further affecting the control stability of hypersonic morphing vehicle.

To enhance the control stability and accuracy of hypersonic morphing vehicles, researchers have investigated various nonlinear control methods to address model nonlinearities and unmodeled dynamics. To ensure agility in highly dynamic environments, much focus has been placed on finite-time, fixed-time, and prescribed-time control methods. Wei *et al*., addressing hypersonic morphing vehicle control system design under conditions like input saturation, parameter uncertainty, and morphing-induced disturbances, utilized a backstepping control framework combined with fixed-time convergence theory to propose an adaptive fixed-time control method [12]. Zhang *et al*., tackling issues such as large parameter perturbations from morphing, difficulty in modeling the morphing process, and complex external disturbances for hypersonic morphing vehicles, combined an extended state observer with finite-time convergence theory to study an attitude controller for a class of variable-sweep vehicle [13]. Zhang *et al*., considering the need for high-performance control and low resource consumption during the morphing flight phase of hypersonic morphing vehicles, proposed a novel event-triggered fast finite-time control method, reducing system resource consumption [14]. Cao *et al*., taking a foldable hypersonic morphing vehicle as the research object and comprehensively considering dynamic changes in aerodynamic and dynamic characteristics due to morphing, along with model uncertainty and external disturbances, investigated fixed-time disturbance observers and fixed-time prescribed performance control [15]. Jiao *et al*., for a hypersonic morphing vehicle with folding wingtips, designed a sliding mode controller incorporating a fuzzy logic system [16]. Liu *et al*., considering the drastic changes and potentially unstable aerodynamic characteristics during morphing, researched extended state observers and sliding mode controllers [17]. Zhang *et al*., for hypersonic morphing vehicles with system uncertainties and limited computational resources, proposed an event-triggered practical prescribed-time control strategy [18]. While the aforementioned methods consider model nonlinearities and unmodeled dynamics, to fully leverage the advantages of morphing vehicles, the optimality of control inputs must also be considered. Therefore, optimal control theory can be integrated into controller design for hypersonic morphing vehicles.

Within Adaptive Dynamic Programming (ADP) methods, the Actor-Critic (AC) structure and neural networks are used to approximate the solution of the Hamilton-Jacobi-Bellman (HJB) equation for nonlinear continuous systems, thereby analytically computing the optimal control input. Bao *et al*., addressing the attitude control problem of a variable-sweep hypersonic morphing vehicle, combined a fuzzy disturbance observer with an ADP control method to obtain real-time approximate optimal feedback control [19]. Li *et al*., introducing an efficient estimator for unknown system dynamics, proposed an adaptive controller based on ADP suitable for hypersonic morphing vehicles under large uncertainties and morphing conditions [20]. Zhao *et al*. proposed an ADP-based control method for the optimal attitude tracking control of hypersonic vehicles with prescribed performance constraints, balancing performance constraints and optimization capabilities under the condition of partially unknown dynamics [21]. However, such control methods are limited by asymptotic or finite-time convergence properties, making it difficult to precisely regulate the system's response characteristics and to accurately design the ratio between the controller bandwidth and the system bandwidth.

Since the finite-time method has a convergence time upper bound that depends on the initial conditions, it is difficult to accurately determine the convergence time when the initial conditions are unknown. Although the fixed-time method has a convergence time that is independent of the initial conditions, its convergence time expression is determined by multiple control parameters and is relatively complex. The prescribed-time control method, on the other hand, has a convergence time that is not only independent of the initial state but can also be determined by a single parameter, allowing the control parameter to be quickly preset according to real-time task requirements. Therefore, in order to address the above problems, this paper introduces Prescribed time control (PTC) technology into an ADP-based control framework. By intuitively adjusting convergence time through a single

control parameter, it enables precise regulation of response characteristics, enhances the control system bandwidth of hypersonic variable-shape vehicles, and achieves superior system agility while maintaining a specified ratio between controller bandwidth and system bandwidth.

In summary, this paper proposes an adaptive preset-time sliding mode control method based on adaptive dynamic programming to address the agile control challenge for hypersonic deformable vehicles during high-magnitude maneuvers. The main contributions are as follows:

1. A non-ambiguous prescribed -time sliding surface based on the hyperbolic sine function has been designed. This sliding surface not only enables the convergence time upper bound to be determined with a single parameter, but also ensures the control law remains continuous and singularity-free throughout the entire time domain. Compared to traditional singularity avoidance strategies employing piecewise logic or higher-order quadratic integration functions, this method significantly reduces computational complexity.

2. An adaptive dynamic reconfiguration (ADP) weak model control scheme for hypersonic vehicles is proposed in this paper. This method effectively utilizes unmolded dynamics in the dynamic regulation of the convergence process, thereby significantly reducing the upper limit of convergence time while effectively enhancing the system's agility.

3. A bandwidth maintenance technique based on adaptive dynamic programming has been developed. This method dynamically optimizes control parameters in real time according to flight conditions, thereby preserving the proportional relationship between controller bandwidth and actuator bandwidth to ensure the system's agile response characteristics.

2. MODEL OF THE HYPERSONIC MORPHING VEHICLE

The hypersonic morphing vehicle studied in this paper is equipped with high-bandwidth three-axis aerodynamic control surfaces serving as control actuators, along with a low-bandwidth morphing mechanism to achieve a variable sweep angle, as shown in Figure **1**.

This paper focuses on the attitude control problem of the hypersonic morphing vehicle. The model describing its rotation about the center of mass can be established using the theorem of moment of momentum:

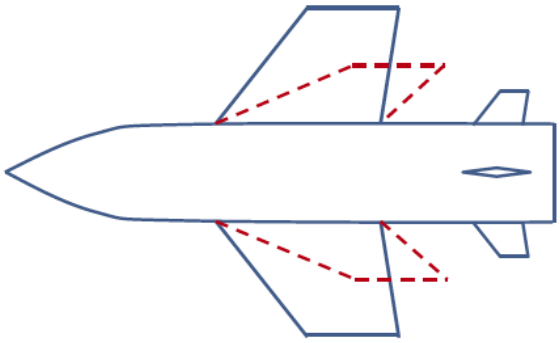

Figure 1: Schematic diagram of a variable-sweep hypersonic vehicle.

$$\begin{cases} \dot{\boldsymbol{\Omega}} = \boldsymbol{R}\omega \\ \boldsymbol{J}\dot{\omega} = -\omega^{\times}\boldsymbol{J}\omega + \boldsymbol{M} + \boldsymbol{M}_{SD} + \boldsymbol{M}_{SG} + \boldsymbol{d} \end{cases} \tag{1}$$

Where $\boldsymbol{\Omega} = \begin{bmatrix} \gamma & \varphi & \psi \end{bmatrix}^{\mathrm{T}}$ is the attitude angle vector; γ is the roll angle; φ is the pitch angle; ψ is the yaw angle; $\omega = \begin{bmatrix} p & q & r \end{bmatrix}^{\mathrm{T}}$ is the angular velocity vector;

$$\omega^{\times} = \begin{bmatrix} 0 & -r & q \\ r & 0 & -p \\ -q & p & 0 \end{bmatrix} \tag{2}$$

p is the roll rate; q is the pitch rate; r is the yaw rate; $\boldsymbol{J}$ is the moment of inertia matrix in the body frame;

$$\boldsymbol{J} = \begin{bmatrix} J_{xx} & 0 & -J_{xz} \\ 0 & J_{yy} & 0 \\ -J_{xz} & 0 & J_{zz} \end{bmatrix} \tag{3}$$

$\boldsymbol{R}$ is the transformation matrix;

$$\boldsymbol{R} = \begin{bmatrix} 1 & \tan\varphi\sin\gamma & \tan\varphi\cos\gamma \\ 0 & \cos\gamma & -\sin\gamma \\ 0 & \dfrac{\sin\gamma}{\cos\varphi} & \dfrac{\cos\gamma}{\cos\varphi} \end{bmatrix} \tag{4}$$

$\boldsymbol{M}_{SD}$ is the additional moment induced by morphing;

$$\boldsymbol{M}_{SD}=2\begin{bmatrix} -p\dot{J}_{1x}-(\dot{p}+qr)J_{1x} \\ m_1S_{1x}(\dot{w}+vp-\mu q)-q\dot{J}_{1y}+(pr-\dot{q})J_{1y} \\ -m_1S_{1x}(\dot{v}+\mu r-wp)-r\left(\dot{J}_{1x}+\dot{J}_{1y}\right)\cdots \\ -\dot{r}\left(J_{1x}+J_{1y}\right)-pq\left(J_{1y}-J_{1x}\right) \end{bmatrix} \tag{5}$$

$\boldsymbol{M}_{SG}$ is the additional moment due to center-of-mass shift;

$$\boldsymbol{M}_{SG}=\begin{bmatrix} -S_{0z}m_0g\cos\varphi\sin\gamma \\ -\left(S_{0x}m_0+2S_{1x}m_1\right)g\cos\varphi\cos\gamma \\ \left(S_{0x}m_0+2S_{1x}m_1\right)g\cos\varphi\sin\gamma \end{bmatrix} \tag{6}$$

$\boldsymbol{d}$ is the unknown disturbance vector caused by external disturbances and unsteady aerodynamic characteristics; μ,v,w is the projection of the vehicle's velocity vector onto the body frame; $S_{ix},S_{iy},S_{iz},i=1,2$ is the projection of the position vector of the left/right wing's center of mass relative to the vehicle's center of mass in the body frame onto the three axes; S_{0x},S_{0y},S_{0z} is the projection of the position vector of the fuselage's center of mass relative to the vehicle's center of mass in the body frame onto the three axes; m_0,m_1 is the mass of the fuselage and wings; J_{ix},J_{iy} is the moment of inertia of each wing about the O_bX_b-axis and O_bY_b-axis of the body frame; $\boldsymbol{M}$ is the aerodynamic moment generated by the fuselage, wings, and control surfaces;

$$\boldsymbol{M}=\boldsymbol{M}_b+\boldsymbol{g}\left(\delta_1,\delta_2\right) \tag{7}$$

$\boldsymbol{M}_b$ is the aerodynamic moment generated by the fuselage; δ_1 is the wing sweep angle, a scalar; δ_2 is the control surface deflection vector.

To more accurately describe the oscillation and overshoot characteristics in the physical system, the morphing mechanism is modeled as a second-order system:

$$\ddot{\delta}_1=-\omega_1^2\delta_1-2\xi_1\omega_1\dot{\delta}_1+\omega_1^2\delta_{1c} \tag{8}$$

where δ_{1c} is the sweep angle command; ω_1 is the bandwidth of the morphing mechanism; ξ_1 is the damping ratio of the morphing mechanism;

The attitude control actuators are modeled as a second-order system:

$$\ddot{\delta}_2=-\omega_2^2\delta_2-2\xi_2\omega_2\dot{\delta}_2+\omega_2^2\delta_{2c} \tag{9}$$

where δ_{2c} is the deflection command vector; ω_2 is the diagonal matrix of actuator bandwidths;

$$\omega_2=\begin{bmatrix} \omega_{21} & \omega_{22} & \omega_{23} \end{bmatrix}^{\mathrm{T}} \tag{10}$$

ω_{21} is the roll surface bandwidth; ω_{22} is the pitch surface bandwidth; ω_{23} is the yaw surface bandwidth; ξ_2 is the diagonal matrix of actuator damping ratios;

$$\xi_2=\begin{bmatrix} \xi_{21} & \xi_{22} & \xi_{23} \end{bmatrix}^{\mathrm{T}} \tag{11}$$

ξ_{21} is the roll surface damping ratio; ξ_{22} is the pitch surface damping ratio; ξ_{23} is the yaw surface damping ratio;

Considering the actuator bandwidths, the model describing the hypersonic morphing vehicle's rotation about the center of mass becomes:

$$\begin{cases} \dot{\boldsymbol{\Omega}}=\boldsymbol{R}\omega \\ \boldsymbol{J}\dot{\omega}=-\omega^{\times}\boldsymbol{J}\omega+\boldsymbol{M}_b+\boldsymbol{g}\left(\delta_1,\delta_2\right)+\boldsymbol{M}_{SD}+\boldsymbol{M}_{SG}+\boldsymbol{d} \\ \ddot{\delta}_1=-\omega_1^2\delta_1-2\xi_1\omega_1\dot{\delta}_1+\omega_1^2\delta_{1c} \\ \ddot{\delta}_2=-\omega_2^2\delta_2-2\xi_2\omega_2\dot{\delta}_2+\omega_2^2\delta_{2c} \end{cases} \tag{12}$$

When the controller output $\boldsymbol{u}$ is the required three-axis moment, the control surface deflection command δ_{2c} can be calculated inversely from the aerodynamic moment. At a given time $t=t_i$, when solving for the deflection command $\delta_{2c}\big|_{t=t_i}$, substituting the morphing command $\delta_{1c}\big|_{t=t_i}$ into the multivariate function $\boldsymbol{g}\left(\delta_{1c},\delta_{2c}\right)$ reduces it to a single-variable function, denoted as $\boldsymbol{g}_{\delta_{1c}}\left(\delta_{2c}\right)$.

$$\boldsymbol{u}=\boldsymbol{M}_b+\boldsymbol{g}\left(\delta_{1c},\delta_{2c}\right)=\boldsymbol{M}_b+\boldsymbol{g}_{\delta_{1c}}\left(\delta_{2c}\right) \tag{13}$$

The deflection command is solved as:

$$\delta_{2c}=\boldsymbol{g}_{\delta_{1c}}^{-1}\left(\boldsymbol{u}-\boldsymbol{M}_b\right) \tag{14}$$

The controller output $\boldsymbol{u}$ is the required three-axis moment. Thus, the model of the hypersonic morphing vehicle's rotation about the center of mass, considering actuator bandwidth, is expressed as:

$$\begin{cases} \dot{\boldsymbol{\Omega}} = \boldsymbol{R}\omega \\ \boldsymbol{J}\dot{\omega} = -\omega^{\times}\boldsymbol{J}\omega + \boldsymbol{M}_b + \boldsymbol{g}\left(\delta_1,\delta_2\right) + \boldsymbol{M}_{SD} + \boldsymbol{M}_{SG} + \boldsymbol{d} \\ \ddot{\delta}_1 = -\omega_1^2\delta_1 - 2\xi_1\omega_1\dot{\delta}_1 + \omega_1^2\delta_{1c} \\ \ddot{\delta}_2 = -\omega_2^2\delta_2 - 2\xi_2\omega_2\dot{\delta}_2 + \omega_2^2\boldsymbol{g}_{\delta_{1c}}^{-1}\left(\boldsymbol{u} - \boldsymbol{M}_b\right) \end{cases} \tag{15}$$

where $\boldsymbol{u} = \boldsymbol{M}_b + \boldsymbol{g}\left(\delta_{1c},\delta_{2c}\right)$;

Define the attitude tracking command and its first derivative as ω_c、$\dot{\omega}_c$. Select the state variables as $\boldsymbol{e}_1 = \boldsymbol{\Omega} - \boldsymbol{\Omega}_c$, $\boldsymbol{e}_2 = \dot{\boldsymbol{\Omega}} - \dot{\boldsymbol{\Omega}}_c$.Substituting into the equation and organizing using the required moment $\boldsymbol{u}$ the attitude tracking control system for the morphing vehicle is obtained as:

$$\begin{cases} \dot{\boldsymbol{e}}_1 = \boldsymbol{e}_2 \\ \dot{\boldsymbol{e}}_2 = \boldsymbol{F} + \boldsymbol{B}\boldsymbol{u} + \Delta\boldsymbol{D} \end{cases} \tag{16}$$

where

$\boldsymbol{B} = \boldsymbol{R}\boldsymbol{J}^{-1}$, $\boldsymbol{F} = \boldsymbol{R}\boldsymbol{J}^{-1}\left(-\omega^{\times}\boldsymbol{J}\omega + \boldsymbol{M}_{SD} + \boldsymbol{M}_{SG}\right)$,

$\Delta\boldsymbol{D} = \boldsymbol{R}\boldsymbol{d} - \ddot{\boldsymbol{\Omega}}_c + \boldsymbol{g}\left(\delta_1,\delta_2\right) - \boldsymbol{g}\left(\delta_{1c},\delta_{2c}\right)$ are the lumped disturbances.

Assumption 1: The lumped disturbance $\Delta\boldsymbol{D} = [\Delta D_1, \Delta D_2, \Delta D_3]^{\mathrm{T}}$ of the system is bounded, i.e., it satisfies $\left|\Delta D_i\right| < D_{mi}\left(i = 1,\ 2,\ 3\right)$.

Remark 1: Due to external disturbances in actual flight, such as uncertain wind fields, wingtip vortices, and aerodynamic coefficient perturbations, they are essentially manifestations of energy. Since the energy in nature is limited, it is reasonable to assume that external disturbances are bounded.

The control objective of this paper is to design a prescribed-time controller with ADP-based compensation, such that the attitude tracking error $\boldsymbol{e}_{1i}\ \left(i = 1,2,3\right)$ converges to a prescribed region within a prescribed time despite unsteady aerodynamic characteristics and unknown disturbances.

3. PRELIMINARY KNOWLEDGE

In this paper, $\mathbb{R}$, $\mathbb{R}^+$, $\mathbb{R}^n$, $\mathbb{R}^{n\times n}$ represent the set of real numbers, positive real numbers, n-dimensional real vector space, and $n\times n$ real matrix space, respectively. $\mathbb{C}(\bullet)$ represents a column vector, $\mathbb{D}(x_i)$ represents a diagonal matrix with x_i as its diagonal elements, $\left|\bullet\right|$ is the absolute value of a real number, $\left\|\bullet\right\|$ is the Euclidean vector norm, and $\mathrm{sign}\left(\bullet\right)$ is the sign function. For any $a\in\mathbb{R}^+$, $x\in\mathbb{R}$ define the function $\mathrm{sig}^a(x) = \mathrm{sign}(x)\left|x\right|^a$. For vectors $\eta\in\mathbb{R}^n\ \eta = [\eta_1,\eta_2,\ldots\eta_n]^{\mathrm{T}}$, define the function $\mathrm{sign}^a(\eta) = [\mathrm{sign}^a(\eta_1),\mathrm{sign}^a(\eta_2),\cdots,\mathrm{sign}^a(\eta_n)]^{\mathrm{T}}$.

Consider the following autonomous system:

$$\dot{\boldsymbol{x}} = \boldsymbol{f}(\boldsymbol{x}(t),\hat{\varphi}),\ \ \boldsymbol{x}(0) = \boldsymbol{x}_0 \tag{17}$$

where $\boldsymbol{x}\in\mathbb{R}^n$ is the state variable, $\boldsymbol{x}_0 = \boldsymbol{x}(0)\in\mathbb{R}^n$ is the initial value. $\hat{\varphi}$ is a tuning parameter of the autonomous system. $\boldsymbol{f}:\mathbb{R}^n\to\mathbb{R}^n$ is a nonlinear function. Assume the solution of the system is $\Phi(t,\boldsymbol{x}_0)$, and the equilibrium point is the origin.

Definition 1: For the autonomous system $\dot{\boldsymbol{x}} = \boldsymbol{f}(\boldsymbol{x}(t),\hat{\varphi})$, if for any $T_c\in\mathbb{R}^+$ and $\mu\in\mathbb{R}^+$, there exists $\hat{\varphi}\in\mathbb{R}^m$ such that when $\forall t > T_c$, the system satisfies $\Phi(t,\boldsymbol{x}_0) < \mu$, then the origin of this autonomous system is prescribed-time stable.

Lemma 1: For $\dot{\boldsymbol{x}} = \boldsymbol{f}(\boldsymbol{x}(t),\hat{\varphi})$, if there exists a positive definite and unbounded Lyapunov function $V(\boldsymbol{x})$ satisfying:

$$\dot{V} \le -\left[1 + V + k^2V^2\right]\left[\frac{2}{\pi}\arctan\left(kV\right)\right]^{1-m} + \Xi \tag{18}$$

Where $m = 1 - \pi/2kT_c$, $k > \pi/T_c$, $T_c > 0$, $\Xi > 0$. Then $V(\boldsymbol{x})$ converges to the origin $V(\boldsymbol{x}) < o$ within the prescribed upper bound of time T_c, $o = \frac{1}{k}\tan\left[\left(2/\pi\right)^{\frac{m-1}{2-m}}\left(k\Xi\right)^{\frac{1}{2-m}}\right]$. The proof of Lemma 1 is as follows.

Proof: $\forall kV > 0$ satisfy the property $kV > \arctan(kV)$. Multiplying both sides of the inequality by $\arctan^{1-m}(kV)$ yields:

$$V\arctan^{1-m}\left(kV\right) \ge \frac{1}{k}\arctan^{2-m}(kV) \tag{19}$$

Substituting the equation (19) into the equation (18), it is easy to derive the following relationship:

$$\dot{V} \le -\frac{1}{k}\left[\frac{2}{\pi}\arctan\left(kV\right)\right]^{2-m} + \Xi \tag{20}$$

Therefore, when $V(\boldsymbol{x}) \geq \frac{1}{k}\tan\left[\left(2/\pi\right)^{\frac{m-1}{2-m}}\left(k\Xi\right)^{\frac{1}{2-m}}\right]$, the convergence rate of $V(\boldsymbol{x})$ strictly satisfies the following relationship:

$$\dot{V} \leq -(1+k^2V^2)\left[\frac{2}{\pi}\arctan\left(kV\right)\right]^m \tag{21}$$

Furthermore, rewriting the equation (21) into differential form yields:

$$\frac{-1}{1+k^2V^2}\mathrm{d}V \geq \left[\frac{2}{\pi}\arctan\left(kV\right)\right]^{1-\pi/2kT_c}\mathrm{d}t \tag{22}$$

Let $s = 2/\pi\arctan\left(kV\right)$, substitute into the above equation, and integrate both sides to obtain:

$$T\left(\boldsymbol{x}_0\right) \leq -\frac{\pi}{2k}\int_{s(\boldsymbol{x}_0)}^{0} s^{\pi/2kT_c-1}\mathrm{d}s = T_c s\left(\boldsymbol{x}_0\right)^{\pi/2kT_c} \leq T_c \tag{23}$$

Since (23) ensures $T(\boldsymbol{x}_0) \leq \lim_{V(\boldsymbol{x}_0)\to\infty} T(\boldsymbol{x}_0) < T_c$, the function $V(\boldsymbol{x})$ can converge to o within the prescribed time T_c. This completes the proof of Lemma 1.

Lemma 2 [22]: For $\sigma \in \mathbb{R}^+$, the following inequality holds:

$$0 \leq |x| - x\tanh\left(\frac{x}{\sigma}\right) \leq k_p\sigma \tag{24}$$

where $k_p = e^{-(k_p+1)}$, i.e., $k_p = 0.2785$.

Lemma 3 [23]: For a nonlinear function of the form $\beta\left(x\right) = \ln\left[1-\tanh^2\left(x\right)\right]$, the following equality holds:

$$\beta(x) = \ln(4) - 2xsign(x) + h_a \tag{25}$$

where h_a is a positive real number with an upper bound.

4. CONTROLLER DESIGN FOR HYPERSONIC MORPHING VEHICLE

To address the control challenge of hypersonic morphing vehicles, this paper proposes a reinforcement-learning-based nonsingular prescribed-time sliding-mode scheme. First, a nonsingular prescribed-time sliding surface built on a hyperbolic-tangent function is devised to furnish the baseline structure that steers the system states to convergence within a user-defined interval. Second, an Actor–Critic reinforcement-learning framework is embedded to compute, in real time, the optimal virtual compensation torque against matched uncertainties. Furthermore, a gain-inversion mapping mechanism translates this optimal torque into an adaptive gain of the sliding-mode controller, thereby optimizing closed-loop performance while rigorously preserving the prescribed-time guarantee. The overall control architecture is depicted in Figure **2**.

A. Non-Singular Prescribed-Time Sliding Surface Design and Basic Control Structure

This section first designs a non-singular sliding surface with prescribed-time convergence and provides the basic structure of the control law based on it. The

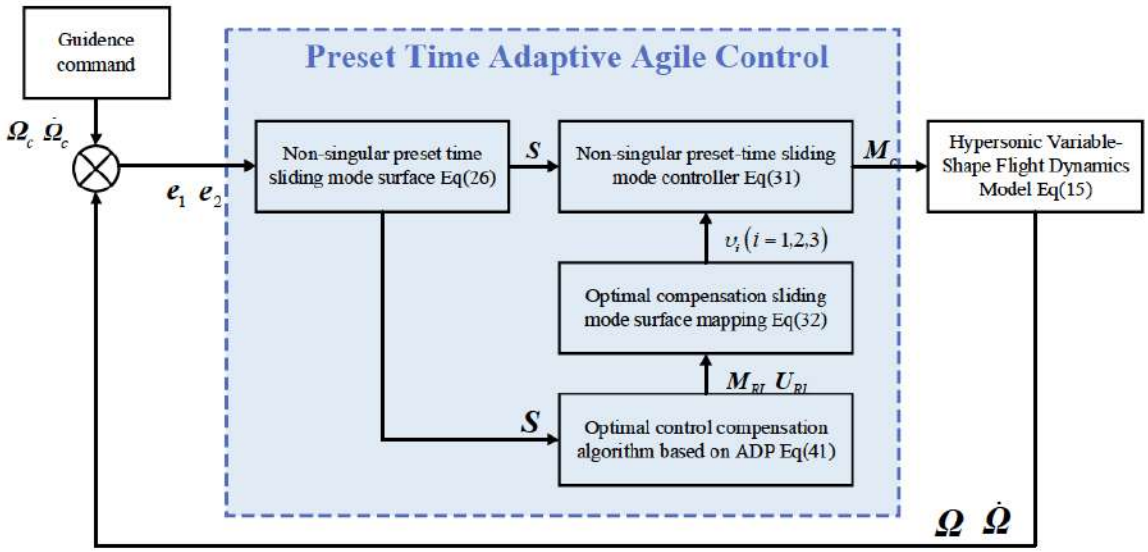

Figure 2: Block diagram of the control scheme for a hypersonic variable-geometry aircraft.

sliding surface structure is as follows:

$$S_i = e_{2i} + \frac{1}{2}e_{1i} + e_{1i}^{-1}\tanh\left[\frac{\alpha(e_{1i})}{\varepsilon}\right]\alpha(e_{1i}) + \frac{e_{1i}}{2}\alpha(e_{1i}) + \frac{k^2 e_{1i}^3}{4}\alpha(e_{1i}) \tag{26}$$

where $\varepsilon > 0$, $\alpha(e_{1i}) = \left[\frac{2}{\pi}\arctan\left(ke_{1i}^2/2\right)\right]^{1-\frac{\pi}{2kT_c}}$.

According to the equation(26), for the tuning of singular terms in the sliding surface, only $e_{1i}^{-1}\tanh\left[\alpha(e_{1i})/\varepsilon\right]\alpha(e_{1i})$ needs attention. Using L'Hôpital's rule for analysis, $\lim_{e_{1i}\to 0} e_{1i}^{-1}\tanh\left[\alpha(e_{1i})/\varepsilon\right]\alpha(e_{1i}) \to 0$. Therefore, the designed sliding surface (26) has no singular terms. Further, taking the first derivativ of S_i yields:

$$\dot{S}_i = \dot{e}_{2i} + \chi_i \ (i = 1,2,3) \tag{27}$$

where

$$\dot{\alpha}(e_{1i}) = \left(1 - \frac{\pi}{2kT_c}\right)\left[\frac{2}{\pi}\arctan\left(\frac{ke_{1i}^2}{2}\right)\right]^{-\frac{\pi}{2kT_c}} \frac{2ke_{1i}e_{2i}}{\left(1+k^2e_{1i}^4/4\right)\pi}$$

$$\chi_i = \left\{e_{1i}^{-1}\left[1 - \tanh^2\left(\frac{\alpha(e_{1i})}{\varepsilon}\right)\right]\right\}\dot{\alpha}(e_{1i})\frac{\alpha(e_{1i})}{\varepsilon} + \left[-e_{1i}^{-2}\tanh\left(\frac{\alpha(e_{1i})}{\varepsilon}\right) + \frac{1}{2} + \frac{3k^2e_{1i}^2}{4}\right]e_{2i}\alpha(e_{1i}) + \left[e_{1i}^{-1}\tanh\left(\frac{\alpha(e_{1i})}{\varepsilon}\right) + \frac{e_{1i}}{2} + \frac{k^2e_{1i}^3}{4}\right]\dot{\alpha}(e_{1i}) + e_{2i}/2$$

The first derivative of the sliding surface contains no singular terms. Taking $e_{2i}\tanh\left[\alpha(e_{1i})/\varepsilon\right]\alpha(e_{1i})/e_{1i}^2$ in the equation (27) as an example, using the infinitesimal theorem $\lim_{x\to 0}\tanh(x) \sim x$、$\lim_{x\to 0}\arctan(x) \sim x$ yields:

$$\begin{aligned}
&\lim_{e_{1i}\to 0} e_{2i}\tanh\left[\alpha(e_{1i})/\varepsilon\right]\alpha(e_{1i})/e_{1i}^2 \\
&= \tanh\left[\lim_{e_{1i}\to 0}\alpha(e_{1i})/\varepsilon\right]\left[\lim_{e_{1i}\to 0}\alpha(e_{1i})\right]e_{2i}/e_{1i}^2 \\
&= \lim_{e_{1i}\to 0}\left(\frac{ke_{1i}^2}{\pi}\right)^{2-\frac{\pi}{kT_c}} e_{2i}/\left(\varepsilon e_{1i}^2\right) \\
&= \lim_{e_{1i}\to 0} e_{1i}^{2-\frac{2\pi}{kT_c}}\left(\frac{k}{\pi}\right)^{2-\frac{2\pi}{kT_c}} e_{2i}/\varepsilon
\end{aligned} \tag{28}$$

From $k > \pi/T_c$, we get $2 - \frac{2\pi}{kT_c} > 0$, thus $\lim_{e_{1i}\to 0} e_{1i}^{2-\frac{2\pi}{kT_c}} \to 0$. Therefore, the first derivative of the sliding surface contains no singular terms. The other terms are analyzed similarly.

Theorem 1: For the prescribed-time sliding surface (26), if the sliding surface variable $|S_i| \le \varepsilon_{si}$, then within the prescribed time T_c the error state variable e_{1i} can converge to the origin $|e_{1i}| \le \tan\left\{\left[k\frac{\varepsilon_{Si}^2/2 + k_p\varepsilon}{(\pi/2)^{m-1}}\right]^{1/(2-m)}\right\}/k$.

Proof: First, define a positive definite and unbounded Lyapunov function $V_i = e_{1i}^2/2$, Taking its derivative and considering Young's inequality transformation yields:

$$\begin{aligned}
&\dot{V}_i = e_{1i}e_{2i} = -\left\{\tanh\left[\frac{\alpha(e_{1i})}{\varepsilon}\right] + \frac{e_{1i}^2}{2} + \frac{k^2e_{1i}^4}{4}\right\}\alpha(e_{1i}) + e_{1i}S_i \\
&-\frac{1}{2}e_{1i}^2 \le \varepsilon_{Si} - \left\{\tanh\left[\frac{\alpha(e_{1i})}{\varepsilon}\right] + \frac{e_{1i}^2}{2} + \frac{k^2e_{1i}^4}{4}\right\}\alpha(e_{1i})
\end{aligned} \tag{29}$$

where taking $\varepsilon_{Si} = \frac{1}{2}S_i^2 > 0$, further derivation using Lemma 2 yields:

$$\begin{aligned}
&\dot{V}_i \le \frac{\varepsilon_{Si}^2}{2} + k_p\varepsilon - \left(1 + \frac{e_{1i}^2}{2} + \frac{k^2e_{1i}^4}{4}\right)\alpha(e_{1i}) \\
&= -\left(1 + V + k^2V^2\right)\left[\frac{2}{\pi}\arctan(kV)\right]^{1-\frac{\pi}{2kT_c}} + \frac{\varepsilon_{Si}^2}{2} + k_p\varepsilon
\end{aligned} \tag{30}$$

From Lemma 1, it is known that the error variable e_{1i} will converge to the origin $\tan\left\{\left[k\frac{\varepsilon_{Si}^2/2 + k_p\varepsilon}{(\pi/2)^{m-1}}\right]^{1/(2-m)}\right\}/k$ within T_c. Theorem 1 is proven.

This paper combines the proposed non-singular prescribed-time sliding surface with the convergence analysis framework of Theorem 1 to design the following basic sliding mode control structure:

$$\begin{cases} \boldsymbol{u}=\boldsymbol{B}^{-1}(\boldsymbol{U}_S+\boldsymbol{U}_{RL}) \\ \boldsymbol{U}_S=\left(\dfrac{-\boldsymbol{S}}{\|\boldsymbol{S}\|^2}-\dfrac{\boldsymbol{S}}{2}-\dfrac{k^2\|\boldsymbol{S}\|^2\boldsymbol{S}}{4}\right)\left[\dfrac{2}{\pi}\arctan\left(\dfrac{k\|\boldsymbol{S}\|^2}{2}\right)\right]^{1-\pi/2kT_c} \\ -\Lambda-\mathbb{D}\left(\lambda_i\right)\ \mathrm{sign}\left(\boldsymbol{S}\right) \\ \boldsymbol{U}_{RL}=-\mathbb{D}\left(\upsilon_i\right)\dfrac{\boldsymbol{S}}{2}\left(\dfrac{2}{\pi}\arctan\left(k\|\boldsymbol{S}\|^2/2\right)\right)^{1-\pi/2kT_c} \end{cases} \tag{31}$$

where $\Lambda=\chi+\boldsymbol{F}$, $\upsilon_i\geq 0$ are variable gain coefficients, $\dot{\lambda}_i(t)=c_i|S_i|$, $c_i\in\mathbb{R}^+$ $(i=1,2,3)$. $\boldsymbol{U}_{RL}$ is the optimization adjustment compensation term, which can provide greater control gain to satisfy better convergence accuracy. This section does not directly give the update formula for the gain coefficients υ_i. Instead, the optimal gains υ_i that balance energy consumption and tracking error will be derived using the Actor-Critic algorithm in the following sections.

B. Online Generation of Optimal Compensation Moment Based on Reinforcement Learning

For the undetermined time-varying gains υ_i in the control law structure of the equation (31), this section constructs a data-driven ADP algorithm. It uses the Actor-Critic learning structure to approximate the system value function online and solve the constrained HJB equation, thereby obtaining the optimal virtual compensation moment $\boldsymbol{M}_{RL}$ against uncertainties. On this basis, to enable the adaptive term $\boldsymbol{U}_{RL}$ in the sliding mode controller to reproduce the optimal strategy output by ADP to the greatest extent, a mapping relationship from the optimal virtual compensation moment $\boldsymbol{M}_{RL}$ to the sliding mode gain υ_i is established based on the vector projection principle, thereby calculating the optimal adaptive gain υ_i in real time.

$$\upsilon_i=\max\left\{0,\frac{-\rho_i\Upsilon(\boldsymbol{S})S_i/2}{\left|\Upsilon(\boldsymbol{S})S_i/2\right|^2+\xi}\right\}\quad(i=1,2,3) \tag{32}$$

where $\xi>0$, $\Upsilon(\boldsymbol{S})=\left(\dfrac{2}{\pi}\arctan\left(k\|\boldsymbol{S}\|^2/2\right)\right)^{1-\pi/2kT_c}$,

$\rho=\boldsymbol{B}\boldsymbol{M}_{RL}=\left[\rho_1,\rho_2,\rho_3\right]^{\mathrm{T}}$. This mechanism maps $\boldsymbol{M}_{RL}$ to the tangential control subspace of the sliding surface, solving for υ_i with the goal of minimizing the approximation error. Considering the non-negativity constraint on gains for prescribed-time control laws and the non-singularity requirement for numerical computation, a truncation operator and regularization term are introduced.

Further, using the optimal compensation $\boldsymbol{M}_{RL}$ to replace $\boldsymbol{B}^{-1}\boldsymbol{U}_{RL}$, in the equation (31), the control law is rewritten as follows[24]:

$$\boldsymbol{M}_c=\boldsymbol{M}_{RL}+\boldsymbol{B}^{-1}\boldsymbol{U}_S \tag{33}$$

To ensure that $\boldsymbol{M}_c$ can satisfy the optimization problem of system error and energy consumption, the following performance index is defined:

$$\begin{aligned} J(\boldsymbol{S},\boldsymbol{M}_{RL})&=\int_t^\infty\left\{\boldsymbol{S}^{\mathrm{T}}\boldsymbol{Q}\boldsymbol{S}+L\left[\boldsymbol{M}_{RL}(\tau)\right]\right\}\mathrm{d}\tau \\ &=\int_t^\infty g(\boldsymbol{S},\boldsymbol{M}_{RL})\mathrm{d}\tau \end{aligned} \tag{34}$$

where $\boldsymbol{Q}$ is a diagonal matrix composed of non-negative real numbers. $L\left[\boldsymbol{M}_{RL}\right]$ measures the consumption of the control law, specifically defined as follows:

$$L(\boldsymbol{M}_{RL})=\int_0^{\boldsymbol{M}_{RL}}2\left[l\tanh^{-1}\left(\frac{z}{l}\right)^{\mathrm{T}}\boldsymbol{R}\right]\mathrm{d}z \tag{35}$$

where $l\in\mathbb{R}^+$ is the actuator control capability, $\boldsymbol{R}$ is a diagonal matrix composed of non-negative real numbers, z is the integration variable, and the integration range is $[0,\boldsymbol{M}_{RL}]$.

Furthermore, define the Lyapunov function related to the performance index as follows, where $\nabla J=\partial J/\boldsymbol{S}$.

$$g(\boldsymbol{S},\boldsymbol{M}_{RL})+\nabla J^{\mathrm{T}}\dot{\boldsymbol{S}}=0 \tag{36}$$

The optimal control quantity $\boldsymbol{M}_{RL}^*$ can be obtained by solving the following HJB equation:

$$g\left(\boldsymbol{S},\boldsymbol{M}_{RL}^*\right)+\nabla J^{*\mathrm{T}}\dot{\boldsymbol{S}}=-\frac{\partial J^*}{\partial t} \tag{37}$$

where J^* is the gradient of the optimal value function, i.e., $J^*=\min_{\boldsymbol{M}_{RL}}\int_t^\infty g(\boldsymbol{S},\boldsymbol{M}_{RL})\mathrm{d}\tau$.

By combining the equations (35) and equations (37) the specific forms of $\boldsymbol{M}_{RL}^*$、$L\left(\boldsymbol{M}_{RL}^*\right)$ can be obtained:

$$\begin{cases} \boldsymbol{M}_{RL}^*=-l\tanh\left(\dfrac{1}{2l}\boldsymbol{R}^{-1}\boldsymbol{B}^{\mathrm{T}}\nabla J^*\right) \\ L\left(\boldsymbol{M}_{RL}^*\right)=-\nabla J^{*\mathrm{T}}\boldsymbol{B}\boldsymbol{M}_{RL}^* \\ +l^2\overline{\boldsymbol{R}}\ln\left[\mathbb{C}(1)-\tanh^2\left(\dfrac{1}{2l}\boldsymbol{R}^{-1}\boldsymbol{B}^{\mathrm{T}}\nabla J^*\right)\right] \end{cases} \tag{38}$$

where $\bar{\boldsymbol{R}}$ is the row vector composed of the diagonal elements of $\boldsymbol{R}$, $L\left(\boldsymbol{M}_{RL}^{*}\right)$ is the integration result of the equation (35).

Simultaneously solving equations (36)~(38) can complete the solution of the control law and performance index. However, $\boldsymbol{M}_{RL}^{*}$ and J^{*} are difficult to express analytically. According to the Weierstrass high-order approximation theorem [25], for any continuous function $Y:\mathbb{U}\to\mathbb{R}$, where $\mathbb{U}$ is a compact set, the function can be approximated by the following network.

$$Y(\boldsymbol{x})=\boldsymbol{W}^{\mathrm{T}}\sigma(\boldsymbol{x})+\varepsilon(\boldsymbol{x}) \tag{39}$$

where, $\sigma\left(\bullet\right)$ is the nonlinear activation function, $\boldsymbol{W}$ is the weight function matrix, $\varepsilon(\boldsymbol{x})$ is the network estimation residual, and when the number of neurons $n\to\infty$, it satisfies $\varepsilon(\boldsymbol{x})\to 0$.

Therefore, this paper adopts the Adaptive Dynamic Programming method with the AC structure for approximate solution, using the Critic network to approximate the optimal performance index function J^{*}, and using the Actor network to generate the optimal control quantity $\boldsymbol{M}_{RL}^{*}$.

$$\begin{cases} J^{*}\left(\boldsymbol{S}\right)=\boldsymbol{W}_{c}^{\mathrm{T}}\sigma\left(\boldsymbol{S}\right)+\varepsilon_{c}(\boldsymbol{S}) \\ \boldsymbol{M}_{RL}^{*}=-l\tanh\left[\dfrac{1}{2l}\boldsymbol{R}^{-1}\boldsymbol{B}^{\mathrm{T}}\left(\nabla\sigma^{\mathrm{T}}\boldsymbol{W}_{a}+\nabla\varepsilon_{a}\right)\right] \end{cases} \tag{40}$$

where $\nabla\sigma=\partial\sigma/\partial\boldsymbol{S}$, $\nabla\varepsilon_{a}=\partial\varepsilon_{a}/\partial\boldsymbol{S}$. $\boldsymbol{W}_{a}$, $\boldsymbol{W}_{c}$ are the ideal weight matrices of the Actor neural network and Critic network. $\sigma\left(\boldsymbol{S}\right)$ is a neural network activation function. $\varepsilon_{c}(\boldsymbol{S})\in\mathbb{R}$ 、 $\varepsilon_{a}(\boldsymbol{S})\in\mathbb{R}$ are the network estimation residuals. Based on the universal approximation property of neural networks for smooth functions on a specified compact set, when $\sigma\left(\boldsymbol{S}\right)$ are finite-dimensional, the network estimation residuals $\varepsilon_{a}(\boldsymbol{S}),\varepsilon_{c}(\boldsymbol{S})$, $\nabla\varepsilon_{a}$ and $\nabla\varepsilon_{c}$ are bounded. And it is assumed that $\left\|\boldsymbol{W}_{a}\right\|,\left\|\boldsymbol{W}_{c}\right\|,\sigma$ and $\nabla\sigma$ are all bounded [26].

Considering that $\boldsymbol{W}_{a}$、$\boldsymbol{W}_{c}$ cannot be obtained, the estimated weights $\hat{\boldsymbol{W}}_{a}$、$\hat{\boldsymbol{W}}_{c}$ of the Actor and Critic neural networks are used to represent the performance index and control quantity:

$$\begin{cases} \hat{J}\left(\boldsymbol{S}\right)=\hat{\boldsymbol{W}}_{c}^{\mathrm{T}}\sigma\left(\boldsymbol{S}\right) \\ \hat{\boldsymbol{M}}_{RL}=-l\tanh\left(\dfrac{1}{2l}\boldsymbol{R}^{-1}\boldsymbol{B}^{\mathrm{T}}\nabla\sigma^{\mathrm{T}}\hat{\boldsymbol{W}}_{a}\right) \end{cases} \tag{41}$$

Simultaneously define the Actor and Critic network weight matrix estimation errors $\tilde{\boldsymbol{W}}_{a}$、$\tilde{\boldsymbol{W}}_{c}$ as:

$$\begin{cases} \tilde{\boldsymbol{W}}_{a}=\boldsymbol{W}_{a}-\hat{\boldsymbol{W}}_{a} \\ \tilde{\boldsymbol{W}}_{c}=\boldsymbol{W}_{c}-\hat{\boldsymbol{W}}_{c} \end{cases} \tag{42}$$

The update of the network weight matrices is based on the Bellman error [24]. Substituting the equation (41) into the Lyapunov function (36) yields the following Bellman error δ_{HJB}.

$$\delta_{HJB}=\boldsymbol{S}^{\mathrm{T}}\boldsymbol{Q}\boldsymbol{S}+L\left(\hat{\boldsymbol{M}}_{RL}\right)+\theta^{\mathrm{T}}\hat{\boldsymbol{W}}_{c} \tag{43}$$

where $\theta=\nabla\sigma\left(B\hat{\boldsymbol{M}}_{RL}+\boldsymbol{U}_{S}+\Lambda\right)$, taking $\bar{\theta}=\theta/\left(\theta^{\mathrm{T}}\theta+1\right)^{2}$.

According to the gradient descent method, the weight update formulas for the Critic network and Actor network in this paper are designed as follows:

$$\dot{\hat{\boldsymbol{W}}}_{a}=-\boldsymbol{A}_{1}\left(\frac{p_{a}}{p_{c}}\boldsymbol{\mathcal{H}}_{\mathrm{gard}}-p_{a}\boldsymbol{\mathcal{L}}_{syn}+\frac{p_{a}w_{a}}{p_{c}}\hat{\boldsymbol{W}}_{a}\right) \tag{44}$$

$$\dot{\hat{\boldsymbol{W}}}_{c}=-\boldsymbol{A}_{2}\left(\bar{\theta}\delta_{HJB}+p_{c}\boldsymbol{\mathcal{L}}_{syn}+w_{c}\hat{\boldsymbol{W}}_{c}\right) \tag{45}$$

where

$$\boldsymbol{\mathcal{L}}_{syn}=\hat{\boldsymbol{W}}_{c}-\hat{\boldsymbol{W}}_{a}\ ,\ \boldsymbol{\mathcal{H}}_{\mathrm{gard}}=-l\nabla\sigma\boldsymbol{B}\Psi\bar{\theta}^{\mathrm{T}}\hat{\boldsymbol{W}}_{c}\ ,$$
$$\Psi=\tanh\left(\frac{\boldsymbol{R}^{-1}\boldsymbol{B}^{\mathrm{T}}\nabla\sigma^{\mathrm{T}}\hat{\boldsymbol{W}}_{a}}{2l}\right)-\tanh\left(\frac{\boldsymbol{R}^{-1}\boldsymbol{B}^{\mathrm{T}}\nabla\sigma^{\mathrm{T}}\hat{\boldsymbol{W}}_{a}}{2l\tau}\right)\ ;$$

The learning rate matrices $\boldsymbol{A}_{1}$、$\boldsymbol{A}_{2}$ are diagonal matrices composed of positive real numbers; where p_{a}, p_{c}, τ, w_{a} and w_{c} all belong to the $\mathbb{R}^{+}$ set, and it is assumed that θ satisfies the Persistent Excitation (PE) condition.

5. STABILITY PROOF OF HYPERSONIC MORPHING VEHICLE CONTROLLER

Given that the proposed integrated control law adopts a coupled architecture of "Non-singular Prescribed-time Sliding Mode and Actor-Critic Reinforcement Learning", this section employs a step-by-step strategy to prove the stability of the control system. Since the compensation term $\boldsymbol{U}_{RL}$ and the gain term υ_{i} of the sliding mode controller are obtained by the reinforcement learning algorithm, the convergence of the neural network weights is a prerequisite for ensuring the physical realizability of the control signals and the non-divergence of the system.

Theorem 2: For the hypersonic morphing vehicle attitude control model, if the near-optimal control law Eq. (41), and the corresponding adaptive weight update algorithms Eq. (44), Eq. (45) proposed in this paper based on the Actor-Critic architecture are adopted, then the weight estimation errors $\tilde{\boldsymbol{W}}_a$ and $\tilde{\boldsymbol{W}}_c$ of the critic network and the actor network are Uniformly Ultimately Bounded (UUB), and the optimal virtual compensation moment $\boldsymbol{M}_{RL}$ output by the Actor network and the gain term υ_i calculated through projection remain bounded within finite time.

The proof of Theorem 2 can be found in Appendix A.

In summary, based on the non-singular sliding mode basic control law constructed in Section 4.1, and combined with the optimal adaptive gain calculated by the ADP algorithm in Section 4.2, the integrated control law for attitude tracking of the hypersonic morphing vehicle is comprehensively given as:

$$\begin{cases} \boldsymbol{M}_c = \boldsymbol{B}^{-1}(\boldsymbol{U}_S + \boldsymbol{U}_{RL}) \\ \boldsymbol{U}_S = -\Upsilon(\boldsymbol{S})\left(\dfrac{\boldsymbol{S}}{\|\boldsymbol{S}\|^2} + \dfrac{\boldsymbol{S}}{2} + \dfrac{k^2\|\boldsymbol{S}\|^2\boldsymbol{S}}{4}\right) - \Lambda \\ -\mathbb{D}(\lambda_i)\operatorname{sign}(\boldsymbol{S}) \\ \boldsymbol{U}_{RL} = -\Upsilon(\boldsymbol{S})\mathbb{D}(\upsilon_i)\dfrac{\boldsymbol{S}}{2} \\ \upsilon_i = \max\left\{0, \dfrac{-\rho_i\Upsilon(\boldsymbol{S})S_i/2}{\left|\Upsilon(\boldsymbol{S})S_i/2\right|^2 + \xi}\right\} \quad (i=1,2,3) \end{cases} \tag{46}$$

This control law aims to use the sliding mode term $\boldsymbol{U}_S$ to ensure the forced convergence of the system state within the prescribed time, while using the adaptive term $\boldsymbol{U}_{RL}$ to optimize the dynamic quality of this approaching process.

Theorem 3: For the hypersonic morphing vehicle attitude control model, under the action of the control law shown in Eq. (46), the sliding variable $S_i\ (i=1,2,3)$ can converge to a range $|S_i| \le \varepsilon_{si} \triangleq \dfrac{1}{k}\tan\left\{\left(\dfrac{2}{\pi}\right)^{\frac{m-1}{2-m}}\left[k\sqrt{2V}\zeta\right]^{\frac{1}{2-m}}\right\}$ within the prescribed time T_c, and the attitude tracking error $e_{1i}\ (i=1,2,3)$ will converge to a range $|e_{1i}| \le \dfrac{1}{k}\tan\left\{\left[k\dfrac{\varepsilon_{Si}^2/2 + k_p\varepsilon}{(\pi/2)^{m-1}}\right]^{1/(2-m)}\right\}$ within $2T_c$.

The proof of Theorem 3 can be found in Appendix B.

Remark 2: The ADP method presented in this paper modulates the conservativeness of response time by leveraging the consistency between unmodeled dynamics and the direction of the dynamic response process. When the unmodeled dynamics are inconsistent with the direction of the response process, the controller is designed conventionally; when the unmodeled dynamics are consistent with the direction of the response process, they are used to provide part of the response torque, thereby speeding up the response and enhancing agility.

Remark 3: T_c specifies the convergence time. k is the sliding mode gain; the larger it is, the stronger the nonlinearity and the faster the initial convergence, but it may cause actuator saturation. It should be selected appropriately according to the task requirements. The larger $\boldsymbol{Q}$ is, the more the reinforcement learning cares about errors, which will drive the compensating torque to increase, allowing the system to converge faster and have smaller steady-state error. However, too large a $\boldsymbol{Q}$ can lead to higher energy consumption. The larger $\boldsymbol{R}$ is, the more reinforcement learning will drive the compensating torque to decrease in order to save energy, but this will make the response slower and the control output smoother. $\boldsymbol{Q}$ and $\boldsymbol{R}$ are core parameters for balancing performance and energy consumption. Adjusting the two should involve a trade-off. $\boldsymbol{A}_1 = 5\boldsymbol{I}_{5\times5}$ and $\boldsymbol{A}_2 = 10\boldsymbol{I}_{5\times5}$ are the learning rate matrix for the Actor and Critic. If the learning rate matrix is too large, it may cause oscillations and fail to converge; if it is too small, learning will be too slow, and optimization results will not be seen for a long time. p_c and p_a are synchronization gains, usually set between 0.1 and 1.0. They help prevent learning failure caused by too large a difference between Actor and Critic weights.

6. SIMULATION OF HYPERSONIC MORPHING VEHICLE

A. Simulation Conditions

The simulation time for the hypersonic morphing vehicle is 20 s. The initial conditions are: angle of attack 10.15°, sideslip angle 0°, Height 35 km, Mach number 8 Ma, with a sweep angle variation of 10°. The principal moments of inertia of the vehicle are 90 kg·m², 200 kg·m², and 200 kg·m². The maximum moment that can be generated by the three-axis virtual control surface deflection is 250 N·m. The actuator frequency is 25 Hz with a damping ratio of 0.7. The aircraft executes a variable sweep maneuver during the period of 0–10 s, with a total sweep angle increment of 10°. The controller parameters in this article are

Table 1: Parameters of Different Control Methods

methods	Parameters
this paper	$T_c=1.5$, $k=1.4\cdot\pi/T_c$, $\varepsilon=0.005$, $\xi=0.0001$, $\boldsymbol{Q}=2\boldsymbol{I}_{3\times3}$, $\boldsymbol{R}=\boldsymbol{I}_{3\times3}$, $\lambda_1=0.05$, $\lambda_1=0.05$, $\lambda_1=0.05$, $c_1=0.05$, $c_1=0.1$, $c_1=0.1$ $\boldsymbol{A}_1=5\boldsymbol{I}_{5\times5}$, $\boldsymbol{A}_1=10\boldsymbol{I}_{5\times5}$, $p_c=0.05$, $p_a=0.15$, $\tau=0.005$, $w_a=0.01$, $w_c=0.01$
Ref. [9]	$\gamma=3.5$, $\delta_\sigma=5^\circ$, $\lambda=0.5$, $\varepsilon=0.0001$, $n_c=4$, $\sigma\in[5^\circ,25^\circ]$
Ref. [13]	$r_z=2$, $\kappa_{z1,2}=10$, $\tau=0.5$, $\kappa_{1\Omega}=0.6$, $\kappa_{2\Omega}=0.5$, $\kappa_{3\Omega}=2$, $\kappa_{4\Omega}=1$, $\eta=0.7$, $r_\Omega=2$, $\beta_{\Omega1}=[100,150,150]^{\mathrm{T}}$, $\beta_{\Omega2}=[300,450,350]^{\mathrm{T}}$, $\delta_\Omega=0.001$, $\theta_\Omega=0.8$, $\beta_{\omega1}=[120,100,90]^{\mathrm{T}}$, $\beta_{\omega2}=[450,350,350]^{\mathrm{T}}$, $\delta_\omega=0.001$, $\theta_\omega=0.8$.

selected as follows: $T_c=1.5$, $k=1.4\cdot\pi/T_c$, $\varepsilon=0.005$, $\xi=0.0001$, $\boldsymbol{Q}=2\boldsymbol{I}_{3\times3}$, $\boldsymbol{R}=\boldsymbol{I}_{3\times3}$, $\lambda_i(i=1,2,3)$ Initial value $\lambda_1=0.05$, $\lambda_1=0.05$, $\lambda_1=0.05$, $c_1=0.05$, $c_1=0.1$, $c_1=0.1$, The base vectors of the actor and critic networks are adjusted in repeated trials to balance the approximation error and the computational burden. They are selected identically as:

$$\sigma(\boldsymbol{S})=\begin{bmatrix}S_1,S_1^2,S_1^3,\tanh(S_1),S_1\tanh(S_1),\\ S_2,S_2^2,S_3^3,\tanh(S_2),S_2\tanh(S_2),\\ S_3,S_3^2,S_3^3,\tanh(S_3),S_3\tanh(S_3),\end{bmatrix} \tag{47}$$

The initial values of $\hat{\boldsymbol{W}}_a$ and $\hat{\boldsymbol{W}}_c$ be set separately 0 and 0.5, network update parameters set to: $\boldsymbol{A}_1=5\boldsymbol{I}_{5\times5}$, $\boldsymbol{A}_1=10\boldsymbol{I}_{5\times5}$, $p_c=0.05$, $p_a=0.15$, $\tau=0.005$, $w_a=0.01$, $w_c=0.01$.

Since the object of this study is a hypersonic vehicle with a variable sweep angle, the proposed control method is compared with those in references [9] and [13], which share the same research object. The parameters of the district linear control controller[9] are selected as $\gamma=3.5$, $\delta_\sigma=5^\circ$, $\lambda=0.5$, $\varepsilon=0.0001$, $n_c=4$, $\sigma\in[5^\circ,25^\circ]$. The parameters of the finite-time control controller in reference [13] are selected as: $r_z=2$, $\kappa_{z1,2}=10$, $\tau=0.5$, $\kappa_{1\Omega}=0.6$, $\kappa_{2\Omega}=0.5$, $\kappa_{3\Omega}=2$, $\kappa_{4\Omega}=1$, $\eta=0.7$, $r_\Omega=2$, $\beta_{\Omega1}=[100,150,150]^{\mathrm{T}}$, $\beta_{\Omega2}=[300,450,350]^{\mathrm{T}}$, $\delta_\Omega=0.001$, $\theta_\Omega=0.8$, $\beta_{\omega1}=[120,100,90]^{\mathrm{T}}$, $\beta_{\omega2}=[450,350,350]^{\mathrm{T}}$, $\delta_\omega=0.001$, $\theta_\omega=0.8$.

B. Simulation Results

Results of the simulation are shown in Figures **3** to **14**.

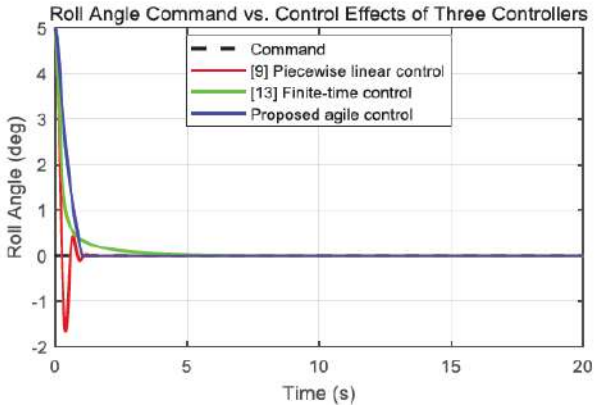

Figure 3: Roll Angle.

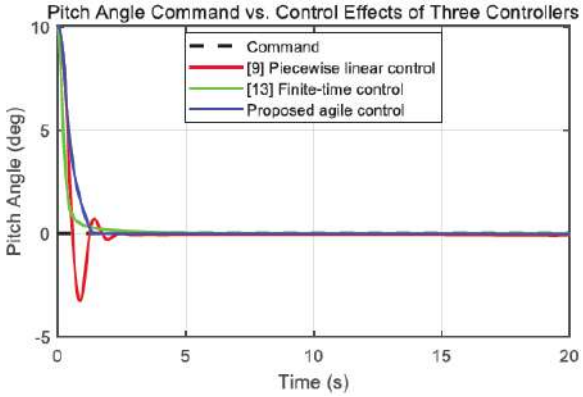

Figure 4: Pitch Angle.

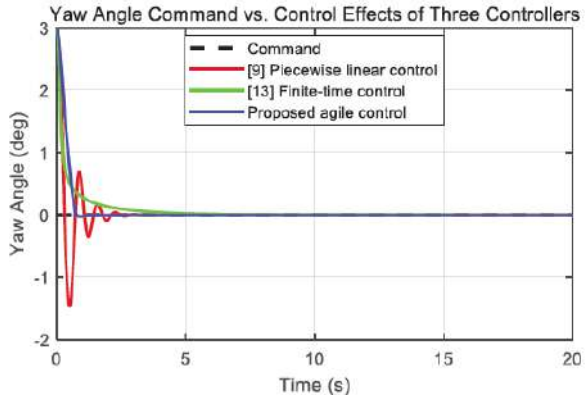

Figure 5: Yaw Angle.

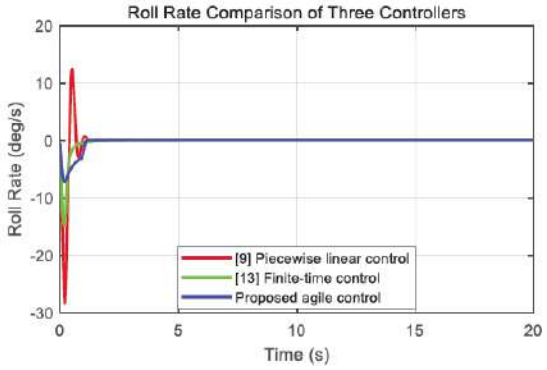

Figure 6: Roll Rate.

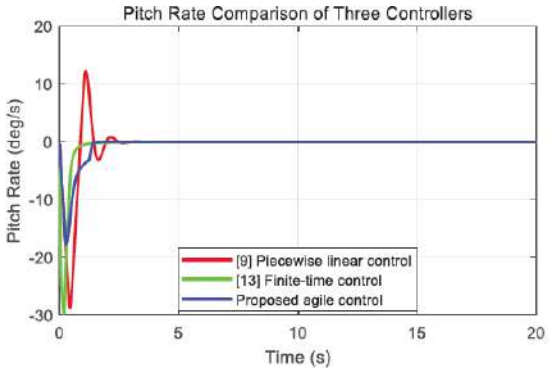

Figure 7: Pitch Rate.

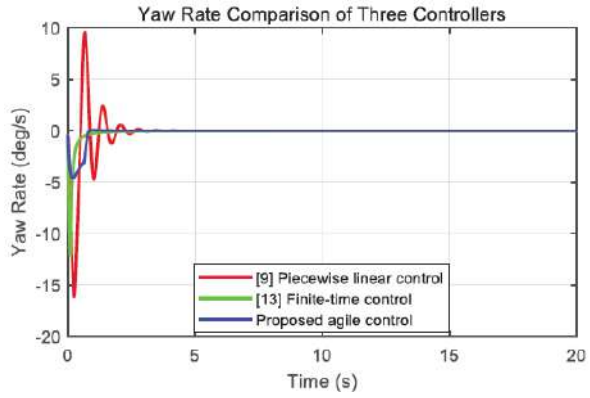

Figure 8: Yaw Rate.

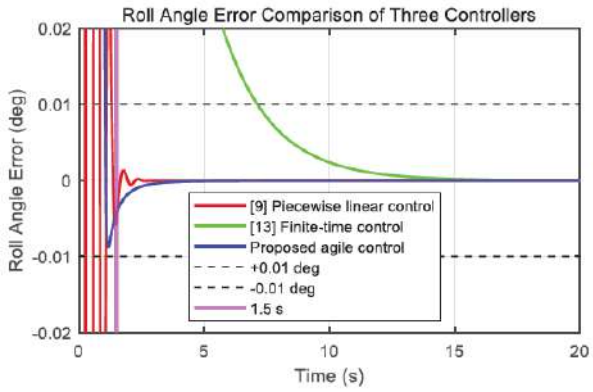

Figure 9: Roll Angle Error.

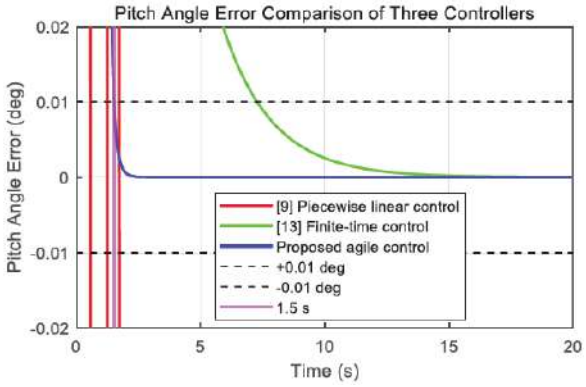

Figure 10: Pitch Angle Error.

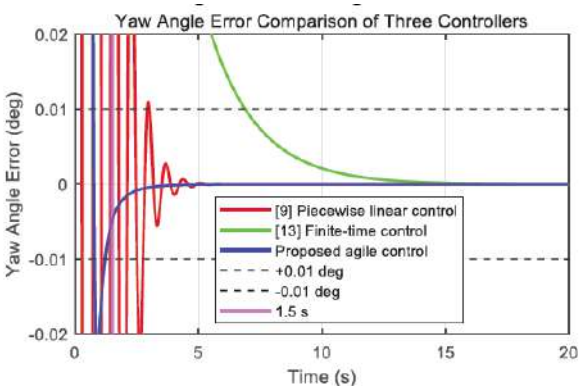

Figure 11: Yaw Angle Error.

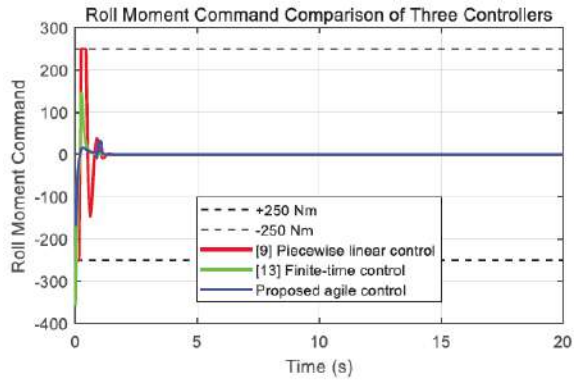

Figure 12: Roll Moment.

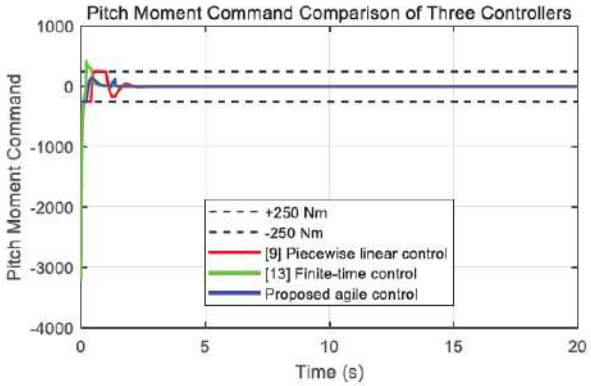

Figure 13: Pitch Moment.

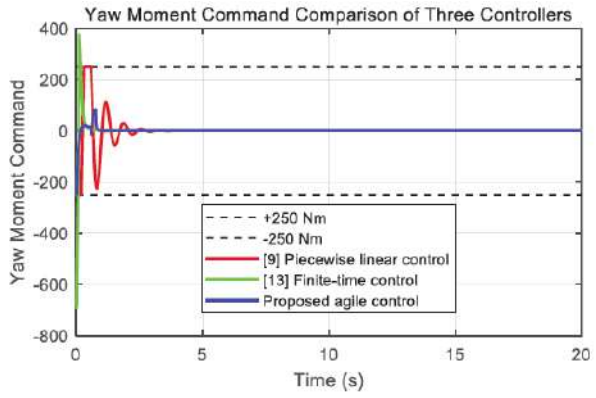

Figure 14: Yaw Moment.

The variations in the aircraft's three-channel attitude angles and angular velocities are shown in Figures **3** to **8**. It can be observed that the proposed control method achieves attitude convergence within the prescribed time while maintaining a smooth dynamic process without significant overshoot. With the preset time convergence mechanism of the controller, the aircraft can strictly follow the time constraints to complete error convergence during the deformation process, even if the response characteristics change, thereby effectively maintaining a reasonable ratio between the controller and system bandwidth.

Furthermore, as demonstrated by the attitude angle deviation curves in Figures **9-11**, the method achieves attitude convergence within 1.5 seconds by leveraging ADP's capability to update unmolded dynamic characteristics. This effectively reduces convergence time conservatism, enhances system agility, and achieves control accuracy within 0.01°.

As shown in the control input curves depicted in Figures **12** to **14**, the control command values designed in this paper are smaller than those of the other two methods. This is attributed to the optimized design of control commands incorporated within the ADP technical indicator function, which effectively reduces energy loss during flight.

7. CONCLUSION

This paper proposes a control method based on adaptive dynamic parameter (ADP) and prescribed time sliding mode to address the agile control challenge for hypersonic morphing vehicles during high-maneuver states. The method utilizes ADP to adapt to unmolded dynamic characteristics, achieving higher control accuracy for hypersonic morphing vehicles with nonlinear and transient aerodynamic properties while maintaining a predetermined proportional relationship between controller bandwidth and vehicle system bandwidth. Simultaneously, a singularity-free prescribed time sliding mode control scheme is designed to precisely regulate convergence time and reduce its upper bound. Finally, simulation comparisons validate the advantages and effectiveness of this approach.

Although the control method in this paper reduces the conservativeness of convergence time to some extent by utilizing unmolded dynamics, the deviation between the preset convergence time and the actual convergence time is still considerable. At the same time, the actuators tend to saturate during deformation maneuvers, which will be the focus of our future research.

COMPETING INTERESTS

The authors declare that there are no conflicts of interest regarding the publication of this paper.

ACKNOWLEDGEMENTS

The authors are grateful to School of Astronautics, Harbin Institute of Technology. This paper is supported by grants from the National Natural Science Foundation of China (No. 62373124).

APPENDIX A

Define the following positive definite and unbounded Lyapunov function:

$$V = \frac{p_c}{2p_a}\tilde{\boldsymbol{W}}_a^{\mathrm{T}}\boldsymbol{A}_1\tilde{\boldsymbol{W}}_a + \frac{1}{2}\tilde{\boldsymbol{W}}_c^{\mathrm{T}}\boldsymbol{A}_2\tilde{\boldsymbol{W}}_c \tag{48}$$

Simultaneously considering Eq. (41) ~ Eq. (45), taking the first derivative of V yields $\dot{V}$:

$$\dot{V} = \frac{p_c}{p_a}\tilde{\boldsymbol{W}}_a^{\mathrm{T}}\boldsymbol{A}_1\dot{\tilde{\boldsymbol{W}}}_a + \tilde{\boldsymbol{W}}_c^{\mathrm{T}}\boldsymbol{A}_2\dot{\tilde{\boldsymbol{W}}}_c \tag{49}$$

Define the following performance error term:

$$B_e = l^2\overline{\boldsymbol{R}}\left\{\begin{array}{l}\ln\left[\mathbb{C}(1)-\tanh^2\left(\frac{1}{2l}\boldsymbol{R}^{-1}\boldsymbol{B}^{\mathrm{T}}\nabla J^*\right)\right] \\ -\ln\left[\mathbb{C}(1)-\tanh^2\left(\frac{1}{2l}\boldsymbol{R}^{-1}\boldsymbol{B}^{\mathrm{T}}\nabla\sigma^{\mathrm{T}}\boldsymbol{W}_a\right)\right]\end{array}\right\} \tag{50}$$

Substituting Eq. (50) into Eq. (37) and integrating, the following relationship is obtained:

$$\begin{aligned}&\boldsymbol{S}^{\mathrm{T}}\boldsymbol{Q}\boldsymbol{S}+\boldsymbol{W}_a^{\mathrm{T}}\nabla\sigma\left(\boldsymbol{U}_S+\Lambda\right)+\varepsilon_H\\&+l^2\overline{\boldsymbol{R}}\ln\left[\mathbb{C}(1)-\tanh^2\left(\frac{1}{2l}\boldsymbol{R}^{-1}\boldsymbol{B}^{\mathrm{T}}\nabla\sigma^{\mathrm{T}}\boldsymbol{W}_a\right)\right]=0\end{aligned}\tag{51}$$

where $\varepsilon_H=\nabla\varepsilon_a{}^{\mathrm{T}}\left(\boldsymbol{U}_S+\chi\right)+B_e+\nabla J^{*\mathrm{T}}\Delta\boldsymbol{D}$ is a bounded HJB error.

Expanding the term $\frac{p_c}{p_a}\tilde{\boldsymbol{W}}_a^{\mathrm{T}}\boldsymbol{A}_1\dot{\hat{\boldsymbol{W}}}_a$ yields:

$$\begin{aligned}&\frac{p_c}{p_a}\tilde{\boldsymbol{W}}_a^{\mathrm{T}}\boldsymbol{A}_1\dot{\hat{\boldsymbol{W}}}_a=\tilde{\boldsymbol{W}}_a^{\mathrm{T}}\left[\mathcal{H}_{\mathrm{gard}}+p_c\boldsymbol{\mathcal{L}}_{syn}+w_a\hat{\boldsymbol{W}}_a\right]=\\&-l\tilde{\boldsymbol{W}}_a^{\mathrm{T}}\nabla\sigma\boldsymbol{B}\Psi\overline{\theta}^{\mathrm{T}}\hat{\boldsymbol{W}}_c-p_c\tilde{\boldsymbol{W}}_a^{\mathrm{T}}\left(\hat{\boldsymbol{W}}_c-\hat{\boldsymbol{W}}_a\right)+w_a\tilde{\boldsymbol{W}}_a^{\mathrm{T}}\hat{\boldsymbol{W}}_a\end{aligned}\tag{52}$$

Similarly, expanding the term $\tilde{\boldsymbol{W}}_c^{\mathrm{T}}\boldsymbol{A}_2\dot{\hat{\boldsymbol{W}}}_c$ yields:

$$\begin{aligned}&\tilde{\boldsymbol{W}}_c^{\mathrm{T}}\boldsymbol{A}_2\dot{\hat{\boldsymbol{W}}}_c=\tilde{\boldsymbol{W}}_c^{\mathrm{T}}\left[\overline{\theta}\delta_{HJB}+p_c\boldsymbol{\mathcal{L}}_{syn}+w_c\hat{\boldsymbol{W}}_c\right]\\&=\tilde{\boldsymbol{W}}_c^{\mathrm{T}}\overline{\theta}\left[\boldsymbol{S}^{\mathrm{T}}\boldsymbol{Q}\boldsymbol{S}+L\left(\hat{\boldsymbol{M}}_{RL}\right)+\theta^{\mathrm{T}}\hat{\boldsymbol{W}}_c\right]\\&+p_c\tilde{\boldsymbol{W}}_c^{\mathrm{T}}\left(\hat{\boldsymbol{W}}_c-\hat{\boldsymbol{W}}_a\right)+w_c\tilde{\boldsymbol{W}}_c^{\mathrm{T}}\hat{\boldsymbol{W}}_c\end{aligned}\tag{53}$$

Substituting Eq. (51) and the definition of θ into Eq. (53) yields the following relationship:

$$\begin{aligned}&\tilde{\boldsymbol{W}}_c^{\mathrm{T}}\boldsymbol{A}_2\dot{\hat{\boldsymbol{W}}}_c=p_c\tilde{\boldsymbol{W}}_c^{\mathrm{T}}\left(\hat{\boldsymbol{W}}_c-\hat{\boldsymbol{W}}_a\right)+w_c\tilde{\boldsymbol{W}}_c^{\mathrm{T}}\hat{\boldsymbol{W}}_c+\\&\tilde{\boldsymbol{W}}_c^{\mathrm{T}}\overline{\theta}\begin{Bmatrix}-\left(\nabla\sigma B\hat{\boldsymbol{M}}_{RL}+\nabla\sigma\boldsymbol{U}_S+\nabla\sigma\chi\right)^{\mathrm{T}}\tilde{\boldsymbol{W}}_c\\-l^2\overline{\boldsymbol{R}}\ln\left[\mathbb{C}(1)-\tanh^2\left(\frac{1}{2l}\boldsymbol{R}^{-1}\boldsymbol{B}^{\mathrm{T}}\nabla\sigma^{\mathrm{T}}\boldsymbol{W}_a\right)\right]\\-l\tilde{\boldsymbol{W}}_a^{\mathrm{T}}\nabla\sigma\boldsymbol{B}\tanh\left(\frac{1}{2l}\boldsymbol{R}^{-1}\boldsymbol{B}^{\mathrm{T}}\nabla\sigma^{\mathrm{T}}\hat{\boldsymbol{W}}_a\right)-\varepsilon_H\\+l^2\overline{\boldsymbol{R}}\ln\left[\mathbb{C}(1)-\tanh^2\left(\frac{1}{2l}\boldsymbol{R}^{-1}\boldsymbol{B}^{\mathrm{T}}\nabla\sigma^{\mathrm{T}}\hat{\boldsymbol{W}}_a\right)\right]\end{Bmatrix}\end{aligned}\tag{54}$$

Using Lemma 2 and Lemma 3 to bound Eq. (54) yields:

$$\begin{aligned}&\tilde{\boldsymbol{W}}_c^{\mathrm{T}}\boldsymbol{A}_2\dot{\hat{\boldsymbol{W}}}_c\le p_c\tilde{\boldsymbol{W}}_c^{\mathrm{T}}\left(\hat{\boldsymbol{W}}_c-\hat{\boldsymbol{W}}_a\right)+w_c\tilde{\boldsymbol{W}}_c^{\mathrm{T}}\hat{\boldsymbol{W}}_c-\tilde{\boldsymbol{W}}_c^{\mathrm{T}}\overline{\theta}\overline{\theta}^{\mathrm{T}}\tilde{\boldsymbol{W}}_c\\&+\tilde{\boldsymbol{W}}_c^{\mathrm{T}}\overline{\theta}\begin{Bmatrix}-\varepsilon_H+l^2\overline{\boldsymbol{R}}\left(\overline{\boldsymbol{h}}_\alpha-\overline{\boldsymbol{h}}_\alpha^*\right)\\-l\hat{\boldsymbol{W}}_a^{\mathrm{T}}\nabla\sigma\boldsymbol{B}\left[\tanh\left(\frac{1}{2l\tau}\boldsymbol{R}^{-1}\boldsymbol{B}^{\mathrm{T}}\nabla\sigma^{\mathrm{T}}\hat{\boldsymbol{W}}_a\right)+\tau_1\right]\\-l\tilde{\boldsymbol{W}}_a^{\mathrm{T}}\nabla\sigma\boldsymbol{B}\tanh\left(\frac{1}{2l}\boldsymbol{R}^{-1}\boldsymbol{B}^{\mathrm{T}}\nabla\sigma^{\mathrm{T}}\hat{\boldsymbol{W}}_a\right)\\+l\boldsymbol{W}_a^{\mathrm{T}}\nabla\sigma\boldsymbol{B}\operatorname{sign}\left(\frac{1}{2l}\boldsymbol{R}^{-1}\boldsymbol{B}^{\mathrm{T}}\nabla\sigma^{\mathrm{T}}\boldsymbol{W}_a\right)\end{Bmatrix}\end{aligned}\tag{55}$$

where $\left\|\overline{\boldsymbol{h}}_\alpha\right\|$, $\left\|\overline{\boldsymbol{h}}_\alpha^*\right\|$ and $\left|\tau_1\right|$ are all bounded.

To simplify the expression, define two bounded vectors $\boldsymbol{f}_1$、$\boldsymbol{f}_2$ as follows:

$$\boldsymbol{f}_1=\begin{Bmatrix}l\nabla\sigma\boldsymbol{B}\tanh\left(\frac{1}{2l\sigma}\boldsymbol{R}^{-1}\boldsymbol{B}^{\mathrm{T}}\nabla\sigma^{\mathrm{T}}\hat{\boldsymbol{W}}_a\right)\\-l\nabla\sigma\boldsymbol{B}\tanh\left(\frac{1}{2l}\boldsymbol{R}^{-1}\boldsymbol{B}^{\mathrm{T}}\nabla\sigma^{\mathrm{T}}\hat{\boldsymbol{W}}_a\right)\end{Bmatrix}\overline{\theta}^{\mathrm{T}}\boldsymbol{W}_c\tag{56}$$

$$\begin{aligned}&\boldsymbol{f}_2=l^2\overline{\boldsymbol{R}}\left(\boldsymbol{h}_\alpha-\boldsymbol{h}_\alpha^*\right)\\&-l\boldsymbol{W}_a^{\mathrm{T}}\nabla\sigma\boldsymbol{B}\left[\tanh\left(\frac{1}{2l\tau}\boldsymbol{R}^{-1}\boldsymbol{B}^{\mathrm{T}}\nabla\sigma^{\mathrm{T}}\hat{\boldsymbol{W}}_a\right)+\tau_1\right]\\&+l\boldsymbol{W}_a^{\mathrm{T}}\nabla\sigma\boldsymbol{B}\operatorname{sign}\left(\frac{1}{2l}\boldsymbol{R}^{-1}\boldsymbol{B}^{\mathrm{T}}\nabla\sigma^{\mathrm{T}}\boldsymbol{W}_a\right)\\&+l\sigma_1\tilde{\boldsymbol{W}}_a^{\mathrm{T}}\nabla\sigma\boldsymbol{B}-\varepsilon_H\end{aligned}\tag{57}$$

Substituting Eq. (52), Eq. (55), and Eq. (56), Eq. (57) into Eq. (49) and organizing yields:

$$\begin{aligned}&\dot{V}\le-\tilde{\boldsymbol{W}}_c^{\mathrm{T}}\overline{\theta}\theta^{\mathrm{T}}\tilde{\boldsymbol{W}}_c+\tilde{\boldsymbol{W}}_c\overline{\theta}\boldsymbol{f}_2+\tilde{\boldsymbol{W}}_a^{\mathrm{T}}\boldsymbol{f}_1\\&+p_c\left(\tilde{\boldsymbol{W}}_a-\tilde{\boldsymbol{W}}_c\right)^{\mathrm{T}}\left(\tilde{\boldsymbol{W}}_a-\tilde{\boldsymbol{W}}_c\right)\\&+w_c\left(\tilde{\boldsymbol{W}}_c^{\mathrm{T}}\boldsymbol{W}_c-\left\|\tilde{\boldsymbol{W}}_c\right\|^2\right)+w_a\left(\tilde{\boldsymbol{W}}_a^{\mathrm{T}}\boldsymbol{W}_a-\left\|\tilde{\boldsymbol{W}}_a\right\|^2\right)\\&\le-\tilde{\boldsymbol{W}}_c^{\top}\overline{\theta}\theta^{\top}\tilde{\boldsymbol{W}}_c+\tilde{\boldsymbol{W}}_c^{\top}\overline{\theta}\boldsymbol{f}_2\\&-\frac{w_a}{2}\left\|\tilde{\boldsymbol{W}}_a\right\|^2-\frac{w_c}{2}\left\|\tilde{\boldsymbol{W}}_c\right\|^2+\overline{\varepsilon}_v\end{aligned}\tag{58}$$

where $\overline{\varepsilon}_v=\tilde{\boldsymbol{W}}_a^{\mathrm{T}}\boldsymbol{f}_1$. Define the generalized variable $\boldsymbol{T}=\left[\tilde{\boldsymbol{W}}_a,\tilde{\boldsymbol{W}}_c\right]^{\mathrm{T}}$. Substituting it into Eq. (58) and organizing yields the following equation:

$$\dot{V}\le-\boldsymbol{T}^{\mathrm{T}}N_1\boldsymbol{T}+\boldsymbol{T}^{\mathrm{T}}N_2+\overline{\varepsilon}_v\tag{59}$$

where $N_1=\operatorname{diag}\left[\frac{w_a}{2}\boldsymbol{I}_{m\times m},\frac{w_c}{2}\boldsymbol{I}_{m\times m}+\overline{\theta}\theta^{\top}\right]$ is a positive definite matrix, $N_2=\left[0,\overline{\theta}\boldsymbol{f}_2\right]^{\mathrm{T}}$. Considering that N_2 is a bounded vector, there exists $\left\|N_2\right\|\le\Lambda_2$, $\Lambda_1=\lambda_{\min}\left(N_1\right)$, $\left|\overline{\varepsilon}_v\right|\le\Lambda_3$, and further setting $\left\|\boldsymbol{T}\right\|=\left[\left\|\tilde{\boldsymbol{W}}_a\right\|,\left\|\tilde{\boldsymbol{W}}_c\right\|\right]^{\mathrm{T}}$, then Eq. (59) satisfies:

$$\dot{V}\le-\Lambda_1\left\|\boldsymbol{T}\right\|^2+\Lambda_2\left\|\boldsymbol{T}\right\|+\Lambda_3\tag{60}$$

Therefore, by solving the quadratic equation, the convergence radius $\overline{r}$ can be obtained. When $\left\|\boldsymbol{T}\right\|>\overline{r}$, $\dot{V}\le0$

$$\overline{r} = \frac{\Lambda_2 + \sqrt{\Lambda_2^2 + 4\Lambda_1\Lambda_3}}{2\Lambda_1} \tag{61}$$

This means $\tilde{\boldsymbol{W}}_a$ 、 $\tilde{\boldsymbol{W}}_c$ are Uniformly Ultimately Bounded (UUB), and $\boldsymbol{W}_a$ is bounded, so the estimated weight $\hat{\boldsymbol{W}}_a$ of the Actor network is bounded. At the same time, since the basis functions are bounded, the compensation moment $\hat{\boldsymbol{M}}_{RL}$ output by the Actor network is bounded. In Eq. (32), since the numerator is bounded and the denominator is always greater than 0, the gain term υ_i is a bounded value at any time. This proves Theorem 2.

APPENDIX B

There exists a reasonable and monotonically increasing gain $\lambda_i \left(i = 1,2,3\right)$, satisfying λ_i is slightly less than $D_{mi} \left(i = 1,2,3\right)$. Define a positive definite and unbounded Lyapunov function.

$$V = \frac{1}{2}\boldsymbol{S}^T\boldsymbol{S} \tag{62}$$

Taking the derivative of Eq. (62) yields:

$$\begin{aligned}
&\dot{V} = \boldsymbol{S}^T\left(\boldsymbol{B}\boldsymbol{u} + \chi + \boldsymbol{F} + \Delta\boldsymbol{D}\right) \\
&= -\left(\frac{\boldsymbol{S}^T\boldsymbol{S}}{\left\|\boldsymbol{S}\right\|^2} + \frac{\boldsymbol{S}^T\boldsymbol{S}}{2} + \frac{k^2\left\|\boldsymbol{S}\right\|^2\boldsymbol{S}^T\boldsymbol{S}}{4}\right)\Upsilon\left(\boldsymbol{S}\right) \\
&-\frac{1}{2}\boldsymbol{S}^T\mathbb{D}\left(\upsilon_i\right)\boldsymbol{S}\Upsilon\left(\boldsymbol{S}\right) \\
&+\boldsymbol{S}^T\Delta\boldsymbol{D} - \boldsymbol{S}^T\mathbb{D}\left(\lambda_i\right)\mathrm{sign}\left(\boldsymbol{S}\right)
\end{aligned} \tag{63}$$

Combining the terms in (63), and according to Theorem 2, $\upsilon_i > 0 \left(i = 1,2,3\right)$, and $\overline{\upsilon} = \min\left\{\upsilon_1, \upsilon_2, \upsilon_3\right\}$, organizing yields:

$$\begin{aligned}
&\dot{V} \le -\left(1 + V + \overline{\upsilon}V + k^2V^2\right)\left(\frac{2}{\pi}\arctan(kV)\right)^{1-m} \\
&+\mathbb{C}^{\mathrm{T}}\left(\left|S_i\right|\right)\mathbb{C}\left(\left|D_{mi}\right| - \lambda_i\right) \\
&\le -\left(1 + V + k^2V^2\right)\left(\frac{2}{\pi}\arctan(kV)\right)^{1-m} + \sqrt{2V}\left\|\varsigma\right\|
\end{aligned} \tag{64}$$

where $\varsigma = \mathbb{C}\left(\left|D_{mi}\right| - \lambda_i\right) \left(i = 1,2,3\right)$; Combining with Lemma 1, the sliding surface variable $\left|S_i\right|$ will converge to $\varepsilon_{si} = \frac{1}{k}\tan\left\{\left(\frac{2}{\pi}\right)^{\frac{m-1}{2-m}}\left[k\sqrt{2V}\left\|\varsigma\right\|\right]^{\frac{1}{2-m}}\right\}$ within the prescribed time T_c. Further combining with Theorem 1, it can be known that within the next T_c time, the tracking error e_{1i} will converge to $\left|e_{1i}\right| \le \frac{1}{k}\tan\left\{\left[k\frac{\varepsilon_{Si}^2/2 + k_p\varepsilon}{(\pi/2)^{m-1}}\right]^{1/(2-m)}\right\}$. This proves Theorem 3.

REFERENCES

[1] Wuyu P, Tao Y, *et al*. Analysis on wing deformation modes of hypersonic morphing aircraft [J]. Journal of National University of Defense Technology 2018; 40(3): 15-21.

[2] Gui C, Guang Y, Hongwei G, *et al*. Review on key technologies for hypersonic morphing aircraft [J]. Aeronautical Science & Technology 2024; 35(05): 28-44.

[3] Chu L, Qi L, Feng G, *et al*. Design, modeling, and control of morphing aircraft: A review[J]. Chinese journal of aeronautics 2022; 35(5): 220-246. https://doi.org/10.1016/j.cja.2021.09.013

[4] Mengdan C, Yong W, Yanan G. Roll Control and Rudder System's Technologic Parameters of Hypersonic Vehicle in Reentry Phase[J]. Space Control and Application 2016; 42(4): 18-23.

[5] Boyi C, Yanbin L, Hao L, *et al*. Stability boundary analysis of hypersonic vehicle with control saturation and bandwidth limitation [J]. Control Theory & Applications 2016; 33(11): 1508-1518.

[6] Wang L, Zhang W, Peng K, *et al*. Adaptive Command Filtered Integrated Guidance and Control for Hypersonic Vehicle with Magnitude, Rate and Bandwidth Constraints[C], MATEC Web of Conferences. EDP Sciences 2018; 151: 05004. https://doi.org/10.1051/matecconf/201815105004

[7] He Z, Yin M, Lu Y. Tensor product model-based control of morphing aircraft in transition process[J]. Proceedings of the Institution of Mechanical Engineers, Part G: Journal of Aerospace Engineering 2016; 230(2): 378-391. https://doi.org/10.1177/0954410015591835

[8] Yue T, Wang L, Ai J. Gain self-scheduled H∞ control for morphing aircraft in the wing transition process based on an LPV model[J]. Chinese Journal of Aeronautics 2013; 26(4): 909-917. https://doi.org/10.1016/j.cja.2013.06.004

[9] Qing W, Huichuan Y, Chaoyang D. Switching LPV control of morphing aircraft based on overlapped parameter area[J]. Journal of Shenyang University of Technology 2013; 35(06): 698-703.

[10] Wu Q, Liu Z, Liu F, *et al*. LPV-based self-adaption integral sliding mode controller with L2 gain performance for a morphing aircraft[J]. IEEE Access 2019; 7: 81515-81531. https://doi.org/10.1109/ACCESS.2019.2923313

[11] Pu J, Zhang Y, Guan Y, *et al*. Recurrent neural network-based predefined time control for morphing aircraft with asymmetric time-varying constraints[J]. Applied Mathematical Modelling 2024; 135: 578-600. https://doi.org/10.1016/j.apm.2024.06.024

[12] Changzhu W, Xin G, Yulong L. Fixed-time Anti-saturation Control for Hypersonic Morphing Flight Vehicle [J]. Journal of Astronautics 2025; 46(4): 731-740

[13] Yuan Z, Wanwei H, Kunfeng L, *et al*. Modeling and finite-time control of hypersonic morphing aircraft [J]. Journal of Beijing University of Aeronautics and Astronautics 2022; 48(10): 1979-1993.

[14] Hao Z, Peng W, Guojian T, *et al*. Event-triggered finite-time control for hypersonic morphing aircraft [J]. Acta Aeronautica et Astronautica Sinica 2023; 44(15): 325-338.

[15] Chengyu C, Fanbiao L, Yuxin L, *et al*. Modeling and fixed-time prescribed-performance control of hypersonic morphing aircraft [J]. Acta Automatica Sinica 2024; 50(3): 486-504.

[16] Jiao X, Fidan B, Jiang J, *et al*. Adaptive mode switching of hypersonic morphing aircraft based on type-2 TSK fuzzy sliding mode control[J]. Science China Information Sciences 2015; 58(7): 1-15. https://doi.org/10.1007/s11432-015-5349-z

[17] Liu H, Zhang Q, Cui L, *et al*. Attitude control of hypersonic morphing aircraft based on incremental backsteping sliding mode[C] 2022 7th International Conference on Intelligent Computing and Signal Processing (ICSP). IEEE 2022; 1324-1331. https://doi.org/10.1109/ICSP54964.2022.9778601

[18] Zhang H, Bao C, Ma W, *et al*. Prescribed-time Attitude Control for Hypersonic Morphing Vehicles Using Morphing Information-Driven Events[J]. IEEE Transactions on Aerospace and Electronic Systems 2024. https://doi.org/10.1109/TAES.2024.3404911

[19] Bao C, Wang P, Tang G. Data-driven based model-free adaptive optimal control method for hypersonic morphing vehicle[J]. IEEE Transactions on Aerospace and Electronic Systems 2022; 59(4): 3713-3725. https://doi.org/10.1109/TAES.2022.3230633

[20] Li S, Shao X, Wang H, *et al*. Adaptive Critic Attitude Learning Control for Hypersonic Morphing Vehicles without Backsteping[J]. IEEE Transactions on Aerospace and Electronic Systems 2025. https://doi.org/10.1109/TAES.2025.3542345

[21] Zhao S, Wang J, Xu H, *et al*. ADP-based attitude-tracking control with prescribed performance for hypersonic vehicles[J]. IEEE Transactions on Aerospace and Electronic Systems 2023; 59(5): 6419-6431. https://doi.org/10.1109/TAES.2023.3276729

[22] Yuan Y, Wang Z, Guo L, *et al*. Barrier Lyapunov functions-based adaptive fault tolerant control for flexible hypersonic flight vehicles with full state constraints[J]. IEEE Transactions on Systems, Man, and Cybernetics: Systems 2018; 50(9): 3391-3400. https://doi.org/10.1109/TSMC.2018.2837378

[23] Modares H, Sistani MBN, Lewis FL. A policy iteration approach to online optimal control of continuous-time constrained-input systems[J]. ISA transactions 2013; 52(5): 611-621. https://doi.org/10.1016/j.isatra.2013.04.004

[24] Vamvoudakis KG, Lewis FL. Online actor–critic algorithm to solve the continuous-time infinite horizon optimal control problem. Automatica 2010; 46: 878-888. https://doi.org/10.1016/j.automatica.2010.02.018

[25] Abu-Khalaf M, Lewis FL. Nearly optimal control laws for nonlinear systems with saturating actuators using a neural network HJB approach. Automatica 2005; 41(5): 779-791. https://doi.org/10.1016/j.automatica.2004.11.034

[26] Wang N, Ying G, Xuefeng Z. Data-driven performance-prescribed reinforcement learning control of an unmanned surface vehicle. IEEE Transactions on Neural Networks and Learning Systems 2021; 32(12): 5456-5467. https://doi.org/10.1109/TNNLS.2021.3056444

Received on 22-11-2025 Accepted on 20-12-2025 Published on 31-12-2025